



# Wide Area Neutral Atmosphere Models for GNSS Applications

Rodrigo F. Leandro, Marcelo C. Santos and Richard B. Langley  
*Geodetic Research Laboratory, Department of Geodesy and Geomatics Engineering  
University of New Brunswick, Fredericton, Canada*

## BIOGRAPHIES

Rodrigo Leandro is a Ph.D. candidate in the Department of Geodesy and Geomatics Engineering, University of New Brunswick (UNB), Canada, where he has been a student since 2004. He holds an M.Sc.Eng. in civil engineering from the University of São Paulo, in São Paulo, Brazil. He has been involved in research in the fields of geodesy and satellite positioning. Mr. Leandro has received a best student paper award from the Canadian Geophysical Union and a student paper award from The Institute of Navigation, both in 2004. In 2006 Mr. Leandro has also received a best presentation award from The Institute of Navigation.

Marcelo Santos is an associate professor in the Department of Geodesy and Geomatics Engineering at UNB. He holds an M.Sc. in geophysics from the National Observatory in Rio de Janeiro, and a Ph.D. in geodesy from UNB. He has been involved in research in the fields of space and physical geodesy, GNSS, and navigation

Richard B. Langley is a professor in the Department of Geodesy and Geomatics Engineering at UNB, where he has been teaching since 1981. He has a B.Sc. in applied physics from the University of Waterloo and a Ph.D. in experimental space science from York University, Toronto. Prof. Langley has been active in the development of GPS error models since the early 1980s and is a contributing editor and columnist for GPS World magazine. He is an ION fellow and shared the ION Burka Award for 2004.

## ABSTRACT

In this work we discuss developments related to neutral atmosphere delay prediction models at UNB. We are introducing a new model, which was designed to provide better predictions for different regions inside a delimited wide area. The goal of this new development is to have a more reliable model for wide area augmentation system users, with some homogeneity in terms of performance

over the area of interest. The approach to create the new wide area neutral atmosphere model for North America (UNBw.na) is comprehensively described and discussed. All result analyses took into consideration the most recent version of UNB models, until now, UNB3m. Results for meteorological parameters prediction showed that the new grid-based model could perform better than a latitude (only) based model (such as UNB3m). The general results do not show a spectacular improvement for the new model, however it is consistently better than its predecessor, and, the improvement for certain regions is more significant than others. Regions where the performance of the old model was not satisfactory had results significantly improved with the new model. A validation of UNBw.na predicted zenith delays was realized using radiosonde-derived delays as reference. This analysis showed that different regions of the continent manifested improvement for the estimations with the new model. Investigation of the performance of both models (UNBw.na and UNB3m) with radiosonde ray-raced delays at a few sample stations showed that UNBw.na generally has a better fit to the yearly behavior of the zenith delays. It was also possible to notice that results from UNBw.na are more consistent between stations at different locations than when using UNB3m. UNBw.na was shown to be consistently better than UNB3m in several aspects, and the adopted procedure for the grid calibration works in an adequate way, resulting in a reliable model.

## INTRODUCTION

Mitigating the neutral atmosphere refraction is a crucial step in GNSS positioning. Also often called tropospheric delays, the neutral atmosphere delays are one of the main sources of measurement errors in GNSS. One usual way to account for these effects is using prediction models. There are also other alternatives for neutral atmosphere delay mitigation, such as the parameterization of the zenith delay in the positioning model, when dual frequency carrier-phase measurements are available. However, even in this case, the parameter is commonly a

residual delay, to correct the initially predicted delay, which means that a prediction model is also needed. In most GNSS applications the prediction of the neutral atmosphere delay is required, even if only for an initial value for which a residual delay is computed.

In this work we discuss developments related to neutral atmosphere delay prediction models at UNB. A number of UNB models have been developed over the past decade. Our latest model version is called UNB3m, and a comprehensive description of it can be found in Leandro et al. [2006].

UNB neutral atmosphere models have their algorithm based on the prediction of surface meteorological parameter values, which are used to compute hydrostatic and non-hydrostatic zenith delays using the Saastamoinen models. The slant delays are determined applying the Niell mapping functions [Niell, 1996] to the zenith delays.

In order to account for the seasonal and regional variation of the neutral atmosphere behavior, meteorological parameters (barometric pressure, temperature, relative humidity, temperature lapse rate ( $\beta$ ) and water vapour pressure height factor ( $\lambda$ )) are used as functions of time (day of year) and position in UNB models. Each meteorological parameter is modeled with two components: the average (mean) and amplitude of a cosine function with one year period. By definition, the origin of the yearly variation is day of year 28. This procedure is similar to the one used in the Niell mapping functions computation.

After average and amplitude of a given meteorological parameter are determined, the parameter value is estimated for the desired day of year according to:

$$X_{\text{doy}} = \text{Avg} - \text{Amp} \cdot \cos\left(\left(\text{doy} - 28\right) \frac{2\pi}{365.25}\right), \quad (1)$$

where  $X_{\text{doy}}$  represents the computed parameter value for day of year (doy), and Avg and Amp are the average and amplitude values respectively. This procedure is followed for each of the previously mentioned five parameters.

Once all parameters are determined for a given position and day of year, the zenith delays are computed according to:

$$d_h^z = \frac{10^{-6} k_1 R}{g_m} \cdot P_0 \cdot \left(1 - \frac{\beta H}{T_0}\right)^{\frac{g}{R\beta}}, \quad (2)$$

and

$$d_{\text{nh}}^z = \frac{10^{-6} (T_m k_2' + k_3) R}{g_m \lambda' - \beta R} \cdot \frac{e_0}{T_0} \cdot \left(1 - \frac{\beta H}{T_0}\right)^{\frac{\lambda' g}{R\beta} - 1}, \quad (3)$$

where

- $d_h^z$  and  $d_{\text{nh}}^z$  are the hydrostatic and non-hydrostatic zenith delays, respectively;
- $T_0$ ,  $P_0$ ,  $e_0$ ,  $\beta$ , and  $\lambda$  are the meteorological parameters computed according to (1);
- $H$  is the orthometric height in meters;
- $R$  is the gas constant for dry air ( $287.054 \text{ J kg}^{-1} \text{ K}^{-1}$ );
- $g_m$  is the acceleration of gravity at the atmospheric column centroid in  $\text{m s}^{-2}$  and can be computed from

$$g_m = 9.784 \left(1 - 2.66 \times 10^{-3} \cos(2\phi) - 2.8 \times 10^{-7} H\right) \quad (4)$$

- $g$  is the standard acceleration of gravity ( $9.80665 \text{ m s}^{-2}$ );
- $T_m$  is the mean temperature of water vapour in K and can be computed from

$$T_m = (T_0 - \beta H) \left(1 - \frac{\beta R}{g_m \lambda'}\right) \quad (5)$$

- $\lambda' = \lambda + 1$  (unitless)
- $k_1$ ,  $k_2'$ , and  $k_3$  are refractivity constants with values  $77.60 \text{ K mbar}^{-1}$ ,  $16.6 \text{ K mbar}^{-1}$  and  $377600 \text{ K}^2 \text{ mbar}^{-1}$ , respectively.

The total slant delay is computed according to

$$d_t = m_h d_h^z + m_{\text{nh}} d_{\text{nh}}^z, \quad (6)$$

where  $m_h$  and  $m_{\text{nh}}$  stand for hydrostatic and non-hydrostatic Niell [1996] mapping functions, respectively.

The procedure above has been used in all versions of UNB models, with the difference between them depending on the way the meteorological parameters ( $T_0$ ,  $P_0$ ,  $e_0$ ,  $\beta$ , and  $\lambda$ ) are determined. Other models have also been based on the same principles, such as the Galileo System Test Bed models developed by European Space Agency [Krueger et al., 2004]. In the case of UNB3m, a look-up table with average and amplitude of the meteorological parameters derived from the U.S. Standard Atmosphere Supplements, 1966 [COESA, 1966] is used. Table 1 shows the UNB3m look-up table.

Table 1. Look-up table of UNB3m model.

Average					
Latitude (degrees)	Pressure (mbar)	Temperature (K)	RH (%)	$\beta$ ( $K m^{-1}$ )	$\lambda$ (unitless)
15	1013.25	299.65	75.0	6.30e-3	2.77
30	1017.25	294.15	80.0	6.05e-3	3.15
45	1015.75	283.15	76.0	5.58e-3	2.57
60	1011.75	272.15	77.5	5.39e-3	1.81
75	1013.00	263.65	82.5	4.53e-3	1.55
Amplitude					
Latitude (degrees)	Pressure (mbar)	Temperature (K)	RH (%)	$\beta$ ( $K m^{-1}$ )	$\lambda$ (unitless)
15	0.00	0.00	0.0	0.00e-3	0.00
30	-3.75	7.00	0.0	0.25e-3	0.33
45	-2.25	11.00	-1.0	0.32e-3	0.46
60	-1.75	15.00	-2.5	0.81e-3	0.74
75	-0.50	14.50	2.5	0.62e-3	0.30

Using the table above, UNB3m is able to predict total zenith delays with an average rms of 4.9 cm [Leandro et al., 2006]. Previous analysis showed that this rms value likely could be improved if more realistic meteorological parameter values were used. Collins and Langley [1998] showed that if UNB models are used with surface-measured meteorological values, they can provide delays with an uncertainty of around 3.5 cm, which would be the performance of a UNB neutral atmosphere model if a perfect surface meteorology model could be implemented. Based on these numbers it is possible to state that a better model than the currently used UNB3m could provide zenith delays with uncertainties between 3.5 and 4.9 cm. One of the reasons why UNB3m is not capable of predicting delays with uncertainty close to 3.5 cm is the fact that the current look-up table is not able to accommodate the differences in the average surface meteorology of different regions. Part of this modeling inability is also due to day-to-day variation of meteorological parameters, however this variation impacts any prediction model, since the modeled behavior is always a smooth curve in time (in our case a cosine curve over the year) while real values are points scattered about this line. Figure 1 shows the day-to-day variation over several years for a station situated at approximately 50° N, 66° W. The blue crosses are the surface measurements of temperature, pressure and water vapour pressure, and the red dots are the predicted values using UNB3m.

The advantage of having a more realistic UNB model with the same functional model is improving the values of the yearly averages and amplitudes, as well as their geographical variation. This is the motivation for creating a new model, capable of describing the behavior of meteorological values more realistically.

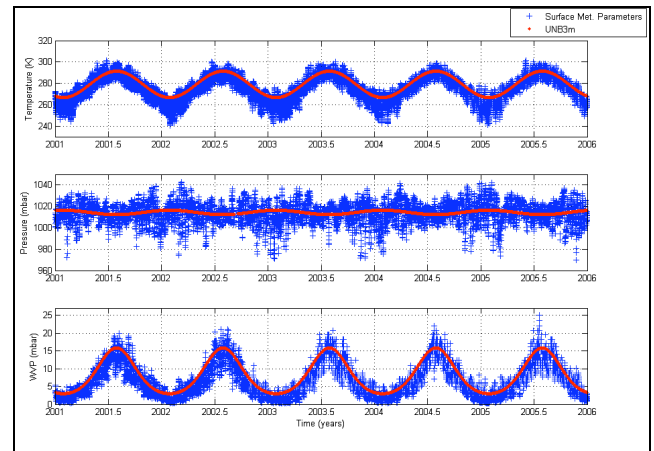


Figure 1. UNB3m surface meteorological parameter predictions compared to measured surface parameter values.

UNB neutral atmosphere models have been used extensively in the context of SBAS (Satellite Based Augmentation Systems). This is the case of CDGPS (Canada-wide Differential GPS), which recommends the use of the UNB3 model by the users, WAAS (Wide Area Augmentation System) and WAAS compatible systems, which use a modified version of UNB3 model running in all WAAS-capable receivers. Although UNB3 is currently the most widely used version of UNB models, the most recent one is UNB3m, which offers a significant improvement in terms of non-hydrostatic zenith delay prediction compared to its predecessor.

In this paper we are introducing a new model, which was designed to provide better predictions for different regions inside a delimited wide area. The goal is to have a more reliable model for wide area augmentation system users, with some homogeneity in terms of performance over the area of interest. These new models are called here wide area neutral atmosphere models, and are treated in more detail in the next section.

## WIDE AREA MODELS

In this section the way the wide area models are generated is reviewed. The first important characteristic of these models is that they keep the same physical assumptions as before (Equations 1 to 5). The key difference in the new approach is the way the surface meteorological values are evaluated, in this case, using a two-dimension grid table instead of a latitude-band look-up table.

One of the first aspects to be taken into account when generating a new model is the data available for its calibration. In this work, we used a data set with world wide hourly measurements of surface temperature, surface dew point temperature and mean sea level barometric pressure. The measurements were made between the years of 2001 and 2005 inclusive. This

dataset was provided by NOAA, from its Integrated Surface Hourly (ISH) Database. Figure 2 shows the global distribution of the ISH database, a total of 17,415 stations.

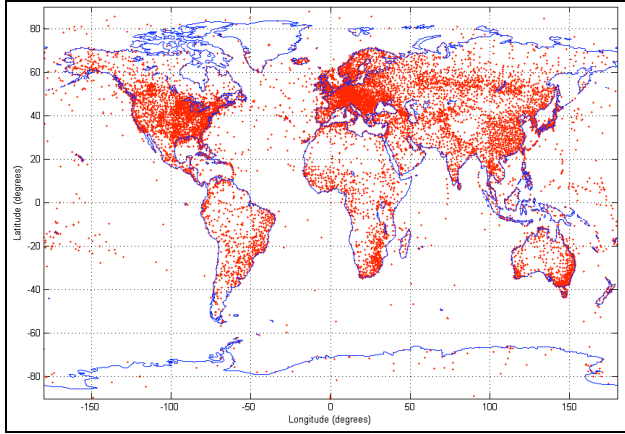


Figure 2. Distribution of ISH Database meteorological stations.

The observations of surface temperature, pressure and dew point temperature are used to calibrate a grid with values of average and amplitude (to be used as in Equation 1) for each of the three parameters (In the case of dew point temperature, it is converted to relative humidity). Near surface temperature lapse rate and water vapor pressure height factor parameters can also be computed if desired. The functional model used for the grid interpolation is very simple, based on the four nearest grid nodes to the observation point (in case of grid calibration) or prediction point (in case of grid use). The value of interest can be computed according to the following formula:

$$X = (1 - p)(1 - q)x_1 + p(1 - q)x_2 + q(1 - p)x_3 + pqx_4, \quad (7)$$

where  $X$  is the computed value (it is either the average or amplitude of one of the modeled parameters),  $x_i$  is the parameter value at grid node  $i$ , and  $p$  and  $q$  are shown in Figure 3.

In Figure 3  $Dx$  and  $Dy$  represent the grid spacing in longitude and latitude, respectively. The black square in the middle of the grid represents the observation point, with coordinates  $\phi_p$  and  $\lambda_p$ . The values for  $p$  and  $q$  can be computed as:

$$p = (\lambda_p - \lambda_1) / Dx, \quad (8)$$

and

$$q = (\phi_p - \phi_1) / Dy, \quad (9)$$

where  $\lambda_p$  and  $\phi_p$  are the longitude and latitude of the point of interest, and  $\lambda_1$  and  $\phi_1$  are the longitude and latitude of grid node 1 (as represented in Figure 3). Therefore  $p$  and  $q$  can assume values between 0 and 1.

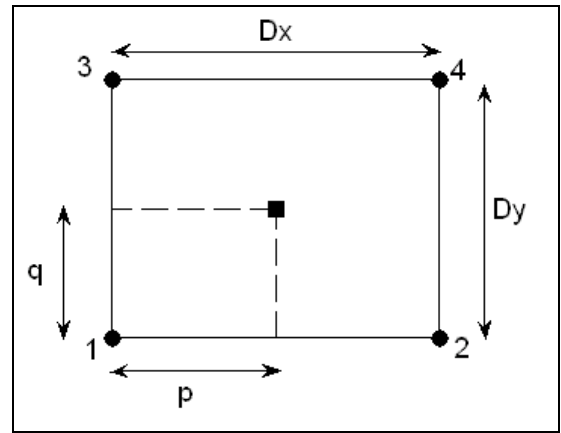


Figure 3. Grid interpolation procedure

Once all surface meteorological parameters for the point of interest are determined using the procedure above, the neutral atmosphere delays can be estimated using Equations 1 to 6. As can be seen, the use of the grid does not bring any significant complexity to the user, however the grid calibration is not a simple procedure.

The establishment of the values for each grid node is carried out in three steps. The first one is the calibration of the temperature ( $T$ ) grid, followed by pressure ( $P$ ) and relative humidity ( $RH$ ) grids. The computation is performed on a station-by-station basis, where all data (all measurements over the observed years) is processed at each station step. For each station, the computation is performed on a year-by-year basis. This procedure is used to improve processing time, since the amount of data is too large to be processed in one single batch adjustment. The general least-squares adjustment model (used in all three grid calibrations) is:

$$\underline{x} = \underline{x}_0 + (\underline{A}^t \underline{P} \underline{A} + \underline{N}_p)^{-1} \underline{A}^t \underline{P} \underline{w}, \quad (10)$$

where  $\underline{x}$  is the vector of updated parameters,  $\underline{x}_0$  is the vector of a-priori parameters (coming from previous updates),  $\underline{A}$  is the design matrix,  $\underline{P}$  is the weight matrix,  $\underline{N}_p$  is the parameter normal matrix (coming from previous updates) and  $\underline{w}$  is the misclosure vector. The parameter normal matrix gets updated at each step, as follows:

$$\underline{N}_{pu} = (\underline{A}^t \underline{P} \underline{A} + \underline{N}_{p0}), \quad (11)$$

where  $\underline{N}_{pu}$  is the updated normal matrix and  $\underline{N}_{p0}$  is the a-priori normal matrix. The updated matrix is used as  $\underline{N}_p$  in (10) at the next parameter update, and then used as  $\underline{N}_{p0}$  in (11), and so on. The observations involved in each update step are the surface meteorological measurements for the current station and current year. The parameters are adjusted for the four nearest grid nodes, using the same functional model as in (7). Therefore the functional model in the adjustment of each grid type (T, P, RH) is built considering (7) plus the relevant formulas (relating interpolated grid values to measurements) for the given parameter type.

The first step, the temperature grid calibration, involves the adjustment of values for mean sea level temperature and optionally the temperature lapse rate. In case the lapse rates are not being adjusted, a-priori values from UNB3m are used as known values. The basic functional model for this step is given by:

$$T = T_0 - \beta H, \quad (12)$$

or, introducing the yearly variation:

$$T = \left( T_{avg} - T_{amp} \cos\left(\frac{doy - 28}{365.25}\right) \right) \dots - H \left( \beta_{avg} - \beta_{amp} \cos\left(\frac{doy - 28}{365.25}\right) \right), \quad (13)$$

where T is the surface temperature measurement,  $T_{avg}$  and  $T_{amp}$  are the mean sea level temperature yearly average and amplitude respectively and  $\beta_{avg}$  and  $\beta_{amp}$  are the temperature lapse rate yearly average and amplitude respectively. Using this function yields the partial derivatives:

$$\frac{\partial T}{\partial T_{avg,i}} = \frac{\partial T}{\partial T_{avg,p}} \frac{\partial T_{avg,p}}{\partial T_{avg,i}} = \frac{\partial T_{avg,p}}{\partial T_{avg,i}}, \quad (14)$$

$$\frac{\partial T}{\partial T_{amp,i}} = \frac{\partial T}{\partial T_{amp,p}} \frac{\partial T_{amp,p}}{\partial T_{amp,i}} = -\cos\left(\frac{doy - 28}{365.25}\right) \frac{\partial T_{amp,p}}{\partial T_{amp,i}}, \quad (15)$$

$$\frac{\partial T}{\partial \beta_{avg,i}} = \frac{\partial T}{\partial \beta_{avg,p}} \frac{\partial \beta_{avg,p}}{\partial \beta_{avg,i}} = -H \frac{\partial \beta_{avg,p}}{\partial \beta_{avg,i}}, \quad (16)$$

$$\frac{\partial T}{\partial T_{amp,i}} = \frac{\partial T}{\partial \beta_{amp,p}} \frac{\partial \beta_{amp,p}}{\partial \beta_{amp,i}} = H \cos\left(\frac{doy - 28}{365.25}\right) \frac{\partial \beta_{amp,p}}{\partial \beta_{amp,i}}, \quad (17)$$

where T is the surface temperature, the subscript p stands for parameters at the point of interest (not to be confused with p representing longitude difference and P representing pressure) and the subscript i stands for parameters at the grid node i. Partial derivatives of point

values with respect to grid node values (e.g.  $\frac{\partial T_{avg,p}}{\partial T_{avg,i}}$ ) are evaluated as follows:

$$\begin{aligned} \frac{\partial X_p}{\partial X_1} &= (1-p)(1-q), & \frac{\partial X_p}{\partial X_2} &= p(1-q) \\ \frac{\partial X_p}{\partial X_3} &= q(1-p) & \text{and} & \frac{\partial X_p}{\partial X_4} = pq \end{aligned} \quad (18)$$

The derivatives in (18) are used in all steps (T, P, RH) of the adjustments of the grids.

The design matrix for the temperature grid calibration is built according to:

$$A = \begin{bmatrix} \frac{\partial T^1}{\partial T_{avg,i}} & \frac{\partial T^1}{\partial T_{amp,i}} & \frac{\partial T^1}{\partial \beta_{avg,i}} & \frac{\partial T^1}{\partial \beta_{amp,i}} \\ \vdots & \vdots & \vdots & \vdots \\ \frac{\partial T^n}{\partial T_{avg,i}} & \frac{\partial T^n}{\partial T_{amp,i}} & \frac{\partial T^n}{\partial \beta_{avg,i}} & \frac{\partial T^n}{\partial \beta_{amp,i}} \end{bmatrix}, \quad (19)$$

where the superscripts 1 and n stand for the observation index (therefore, A is a matrix with n rows, for n observations). In case the lapse rates are not being adjusted, the design matrix has only two columns (the first two of Equation 19). The misclosure vector is computed according to:

$$w = T - T', \quad (20)$$

where T is the measured surface temperature and T' is the evaluated surface temperature according to (13).

After the temperature grid is calibrated (meaning values of  $T_{avg}$ ,  $T_{amp}$ ,  $\beta_{avg}$  and  $\beta_{amp}$  have been established for all of the grid nodes) the relative humidity grid can be adjusted, or alternatively the pressure grid, which does not depend on temperature or relative humidity.

The ISH database provides hourly measurements of MSL barometric pressure, no matter the height of the meteorological station. The consequence is that the pressure measurements have no relation with any lapse rate type parameter. In case of surface pressure, the respective lapse rate would be  $\beta$ , assuming the height variation of pressure relates to the temperature variation of pressure according to:

$$P_s = P_0 \left( 1 - \frac{\beta H}{T_0} \right)^{\frac{g}{R\beta}} = P_0 \left( \frac{T}{T_0} \right)^{\frac{g}{R\beta}}, \quad (21)$$

where  $P_s$  stands for surface pressure. However, because the pressure measurements are related to mean sea level, the function model of the pressure grid adjustment becomes:

$$P = P_{\text{avg}} - P_{\text{amp}} \cos\left(\frac{\text{doy} - 28}{365.25}\right), \quad (22)$$

where  $P$  is the MSL pressure measurement and the yearly variation parameters ( $P_{\text{avg}}$  and  $P_{\text{amp}}$ ) are similar to the ones previously used for  $T$  and  $\beta$  (Eq. 13). Partial derivatives are also evaluated similarly to (14) and (15):

$$\frac{\partial P}{\partial P_{\text{avg},i}} = \frac{\partial P}{\partial P_{\text{avg},p}} \frac{\partial P_{\text{avg},p}}{\partial P_{\text{avg},i}} = \frac{\partial P_{\text{avg},p}}{\partial P_{\text{avg},i}}, \quad (23)$$

$$\frac{\partial P}{\partial P_{\text{amp},i}} = \frac{\partial P}{\partial P_{\text{amp},p}} \frac{\partial P_{\text{amp},p}}{\partial P_{\text{amp},i}} = -\cos\left(\frac{\text{doy} - 28}{365.25}\right) \frac{\partial P_{\text{amp},p}}{\partial P_{\text{amp},i}}. \quad (24)$$

The design matrix then yields:

$$A = \begin{bmatrix} \frac{\partial P^1}{\partial P_{\text{avg},i}} & \frac{\partial P^1}{\partial P_{\text{amp},i}} \\ \vdots & \vdots \\ \frac{\partial P^n}{\partial P_{\text{avg},i}} & \frac{\partial P^n}{\partial P_{\text{amp},i}} \end{bmatrix}, \quad (25)$$

and the misclosure vector is computed according to:

$$w = P - P', \quad (26)$$

where  $P$  is the measured MSL pressure and  $P'$  is the evaluated MSL pressure according to (22).

The calibration of the relative humidity grid involves a little more complexity than the previous ones because (1) it depends on temperature and pressure grids; and (2) the measurements are surface dew point temperature, but the height variation is modeled for water vapor pressure and the yearly variation is modeled for relative humidity. The transformation between these three types of parameters needs to be carried out and incorporated in the functional model for the grid adjustment. The first part of the functional model is the computation of the MSL relative humidity, done similarly to  $T$  and  $P$ :

$$RH_0 = RH_{\text{avg}} - RH_{\text{amp}} \cos\left(\frac{\text{doy} - 28}{365.25}\right), \quad (27)$$

where  $RH_0$  stands for MSL relative humidity and the subscripts avg and amp stand for yearly average and amplitudes, respectively. The relative humidity has then to be transformed in water vapour pressure, which will be

used for height variation modeling. The relation between the two (relative humidity and water vapour pressure) is given by the following equation (according to IERS conventions 2003):

$$e_0 = RH_0 \cdot es_0 \cdot f_{w,0}, \quad (28)$$

where  $e_0$  is the MSL water vapour pressure,  $es_0$  is the saturation water vapour pressure and  $f_{w,0}$  is the enhancement factor (both for MSL). Values for  $e_{s,0}$  and  $f_{w,0}$  can be computed according to:

$$e_{s,0} = 0.01 \cdot \exp(1.2378847 \times 10^{-5} T_0^2 \dots - 1.9121316 \times 10^{-2} T_0 + 33.93711047 \dots, - 6.3431645 \times 10^3 T_0^{-1}) \quad (29)$$

and

$$f_{w,0} = 1.00062 + 3.14 \times 10^{-6} P_0 \dots + 5.6 \times 10^{-7} (T_0 - 273.15)^2 \quad (30)$$

The relation between MSL and surface water vapour pressure is expressed using the same physical assumption as in (3), as follows:

$$e = e_0 \left(1 - \frac{\beta H}{T_0}\right)^{\frac{\lambda' g}{R\beta}}, \quad (31)$$

where  $e$  stands for surface water vapour pressure. The last part of the functional model is the relation between  $e$  and dew point temperature, which can be derived from basic thermodynamic laws, resulting in:

$$e = es(T_d) \cdot f_{w,s}, \quad (32)$$

where  $es(T_d)$  is the saturation water vapour pressure for the dew point temperature  $T_d$ , and can be computed from (29) substituting  $T_d$  for  $T_0$ , and  $f_{w,s}$  can be computed from (30) substituting in values of pressure and surface temperature. After putting (28) to (32) together, the complete functional model “observation equation” for relative humidity calibration becomes:

$$es(T_d) = RH_0 \cdot es_0 \cdot \frac{f_{w,0}}{f_{w,s}} \cdot \left(1 - \frac{\beta H}{T_0}\right)^{\frac{\lambda' g}{R\beta}}, \quad (33)$$

Where, as before, subscripts s and 0 stand for surface and MSL values, respectively. In order to introduce average

and amplitude for the modeled parameters in (34),  $RH_0$  is replaced by the right hand side of (28) and  $\lambda'$  is replaced by:

$$\lambda' = \lambda'_{avg} - \lambda'_{amp} \cos\left(\frac{\text{doy} - 28}{365.25}\right). \quad (34)$$

The partial derivatives can then be evaluated as:

$$\frac{\partial e_s(T_d)}{\partial RH_{avg}} = \frac{\partial e_s(T_d)}{\partial RH_{avg,p}} \frac{\partial RH_{avg,p}}{\partial RH_{avg,i}} = \dots \quad (35)$$

$$e_{s,0} \cdot \frac{f_{w,0}}{f_{w,s}} \left(1 - \frac{\beta H}{T_0}\right)^{\frac{g\lambda'}{R\beta}} \cdot \frac{\partial X_p}{\partial X_i}$$

$$\frac{\partial e_s(T_d)}{\partial RH_{aamp}} = \frac{\partial e_s(T_d)}{\partial RH_{aamp,p}} \frac{\partial RH_{aamp,p}}{\partial RH_{aamp,i}} = \dots \quad (36)$$

$$-\cos\left(\frac{\text{doy} - 28}{365.25}\right) \cdot \frac{\partial e_s(T_d)}{\partial RH_{avg}}$$

$$\frac{\partial e_s(T_d)}{\partial \lambda'_{avg}} = \frac{\partial e_s(T_d)}{\partial \lambda'_{avg,p}} \frac{\partial \lambda'_{avg,p}}{\partial \lambda'_{avg,i}} = \dots \quad (37)$$

$$RH_0 \cdot e_{s,0} \cdot \frac{f_{w,0}}{f_{w,s}} \left(1 - \frac{\beta H}{T_0}\right)^{\frac{g\lambda'}{R\beta}} \cdot \frac{g}{R\beta} \dots$$

$$\ln\left(1 - \frac{\beta H}{T_0}\right) \cdot \frac{\partial X_p}{\partial X_i}$$

and

$$\frac{\partial e_s(T_d)}{\partial \lambda'_{aamp}} = \frac{\partial e_s(T_d)}{\partial \lambda'_{aamp,p}} \frac{\partial \lambda'_{aamp,p}}{\partial \lambda'_{aamp,i}} = \dots \quad (38)$$

$$-\cos\left(\frac{\text{doy} - 28}{365.25}\right) \cdot \frac{\partial e_s(T_d)}{\partial \lambda'_{avg}}$$

and the design matrix becomes:

$$A = \begin{bmatrix} \frac{\partial e_s(T_d)}{\partial RH_{avg,i}} & \frac{\partial e_s(T_d)}{\partial RH_{amp,i}} & \frac{\partial e_s(T_d)}{\partial \lambda'_{avg,i}} & \frac{\partial e_s(T_d)}{\partial \lambda'_{amp,i}} \\ \vdots & \vdots & \vdots & \vdots \\ \frac{\partial e_s(T_d)}{\partial RH_{avg,i}} & \frac{\partial e_s(T_d)}{\partial RH_{amp,i}} & \frac{\partial e_s(T_d)}{\partial \lambda'_{avg,i}} & \frac{\partial e_s(T_d)}{\partial \lambda'_{amp,i}} \end{bmatrix} \quad (40)$$

The misclosure vector is computed according to:

$$w = e_s(T_d) - e_s(T_d), \quad (41)$$

where  $e_s(T_d)$  is computed according to (30) using the measured dew point temperature and  $e_s(T_d)$  is evaluated

using (34). In case the lapse rate parameter ( $\lambda'$ ) is not being adjusted, the design matrix has only its two first columns (related to RH) and  $\lambda'$  values from UNB3m are used as known values.

## WIDE AREA MODEL FOR NORTH AMERICA – UNBw.na

In this section the creation of a model for North America using the previously described procedure is discussed. The model is called UNBw.na, where w stands for wide area and na stands for North America. The grid was defined between latitudes 0 and 90 degrees, and longitudes between -180 and -40 degrees, with spacing of 5 degrees in the two directions. Figure 4 shows the North American grid.

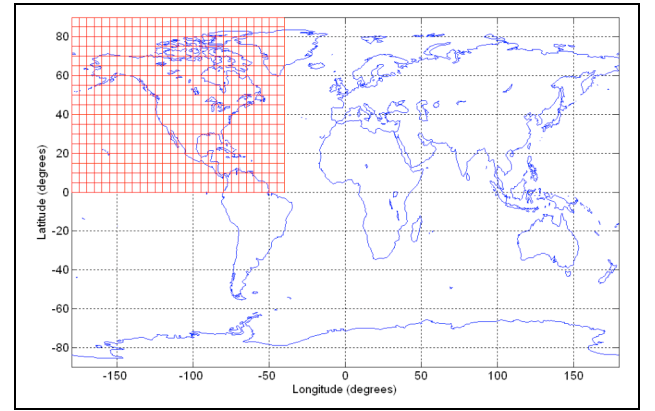


Figure 4. UNBw.na grid (red lines).

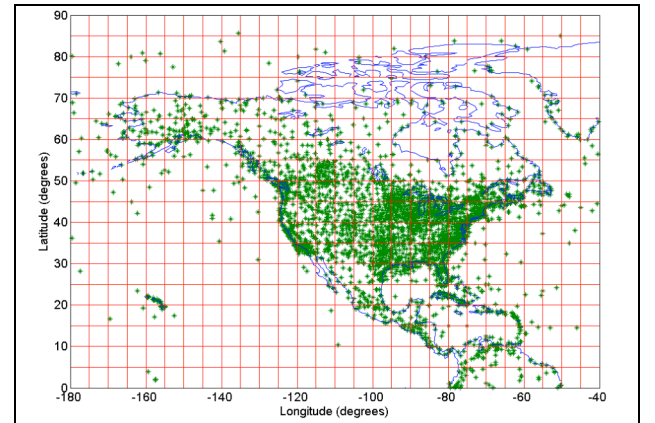


Figure 5. Distribution of meteorological stations over the UNBw.na grid

The grid is first initialized with UNB3m values, and then the grid node values are updated (adjusted) using the previously described approach. The initialization of the grid is fundamental for its adjustment because meteorological stations in the ISH database do not cover every cell of the grid. In this case, the grid node receives no update, and the consequence is a value equal to UNB3m's. The stations to be used in the calibration of the

grid were chosen simply taking database stations within the grid (In this case a total of around 4000 stations). Figure 5 shows the distribution of meteorological stations over the grid.

In order to access the grid adjustment, 400 stations were randomly separated from the dataset to be used as control stations. This data was not used in the grid calibration, and after each adjustment step they were used to check results obtained for temperature, pressure and water vapour pressure. Figure 6 shows the distribution of the control stations (black dots) and calibration stations (green crosses).

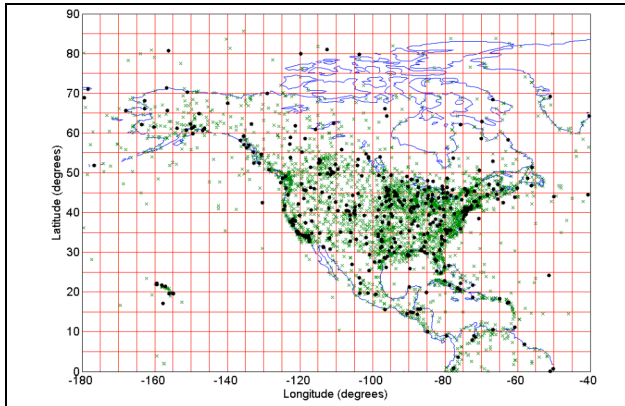


Figure 6. Distribution of the control stations (black dots) and the calibration stations (green crosses).

As shown in the previous section, the temperature lapse rate and water vapour pressure height factor could be calibrated or not. The two approaches were tested for this data set, and it turned out that the model provided slightly better results when lapse rates from UNB3m were used as known and were not recalibrated. One of the reasons which could have caused this is the fact that stations within a given grid cell have similar heights, which causes difficulties in the decorrelation between temperature or water vapour pressure and their lapse rate parameters. Figure 7 shows the height (represented by color) of the stations, where it is possible to notice that apart from a few cells, the height of stations inside cells is usually very similar.

The following results are presented only for the case when the lapse rates were not calibrated. Figure 8 shows a representation of average MSL temperature given by UNB3m and UNBw.na for all grid nodes of the model. It is possible to notice that UNBw.na shows lower temperatures for some northern regions. Also, for some regions, the temperature does not quite follow a variation dependent on latitude only. The two grids are practically the same for grid nodes outside the continent (over seas) because there is not enough data for grid calibration in these regions (see Figure 5), and UNB3m values from the

initialization are almost unmodified by the calibration process.

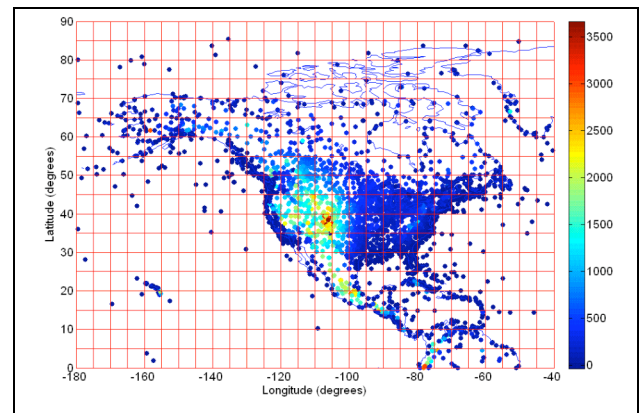


Figure 7. Height (in meters – represented by color) of the meteorological stations.

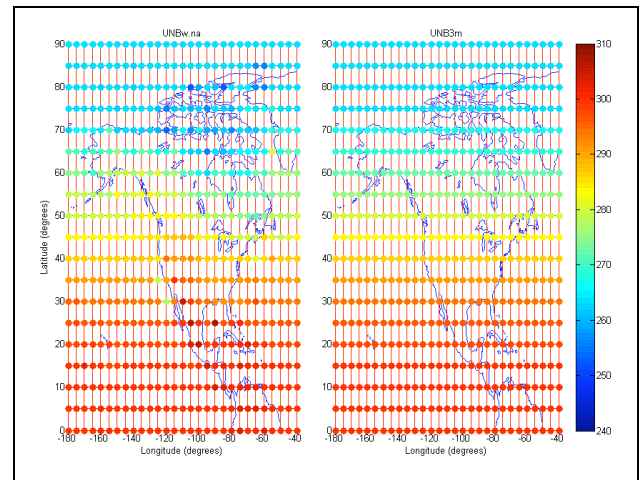


Figure 8. Average MSL temperature given by UNB3m and UNBw.na, in kelvins.

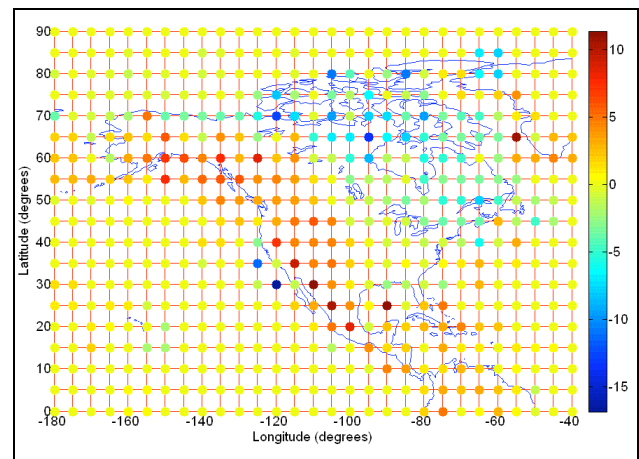


Figure 9. MSL temperature difference between UNBw.na and UNB3m, in kelvins.

Figure 9 shows the difference between the two models, in the sense of UNBw.na-UNB3m. It can be seen that

UNBw.na provides higher temperatures over the western part of North America, and lower temperatures for land mass with higher latitudes over the eastern part of the continent.

With the estimation of temperature for control stations is possible to check if these differences are bringing improvement to the model or not. Figure 10 shows the biases encountered when estimating temperatures for control stations, using the two models, in the sense modeled value – observed value. It is possible to notice that there is a significant improvement in estimation for stations in the western part of North America, matching with differences of grid values (Figure 9) for the same region. It can also be noticed that UNB3m slightly overestimates the temperature for a localized region near the east coast. In terms of UNBw.na one can see that there is no trend related to longitude variation.

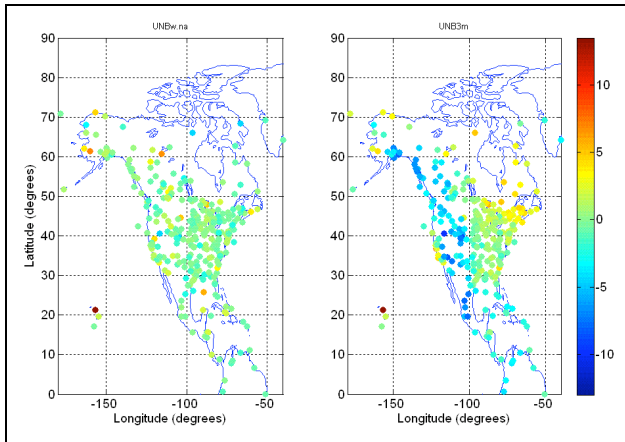


Figure 10. Biases encountered when estimating temperature for control stations, in kelvins.

General statistics for temperature estimation errors for the two models with respect to control station values can be seen in Table 2, where it is possible to notice the overall improvement brought by UNB3w.na in terms of temperature estimation. The values in Table 2 (and similar tables for pressure and water vapour) were computed using one value (bias, standard deviation and rms) per station, regardless the number of measurements available for each station. There is a significant improvement in the bias of the model (91%), showing that UNB3m generally underestimates the mean temperature. This systematic behavior is dominated by the temperature underestimation over the western part of the continent.

Table 2. General statistics for temperature estimation errors (all values in kelvins).

	Bias	Std. Dev.	RMS
UNBw.na	0.06	5.57	5.80
UNB3m	-0.68	6.04	6.80

The results of the following step in grid calibration (the pressure grid) is shown in Figure 11, where it can be noticed that UNBw.na also does not follow the latitude (only) dependence of UNB3m. Figure 12 shows the difference between average MSL pressure of the two models, in the sense of UNBw.na-UNB3m. It can be noticed that the major differences are encountered in regions situated in the northwest, northeast and southern parts of the continent. Differences vary up to around 10 mbar, which means a difference of around 2 cm in hydrostatic delay estimation (according to Equation 2, if we consider a point at MSL, the delay rate with respect to pressure is around 0.0022 m/mbar). Figure 13 shows the biases of UNB3m and UNBw.na when estimating pressure for the control stations, where it can be seen that UNBw.na performs better than UNB3m for the regions where greater differences are found. Overall, the bias plot of UNBw.na is greener than UNB3m's, which means it is usually closer to zero (green is zero on the color scale).

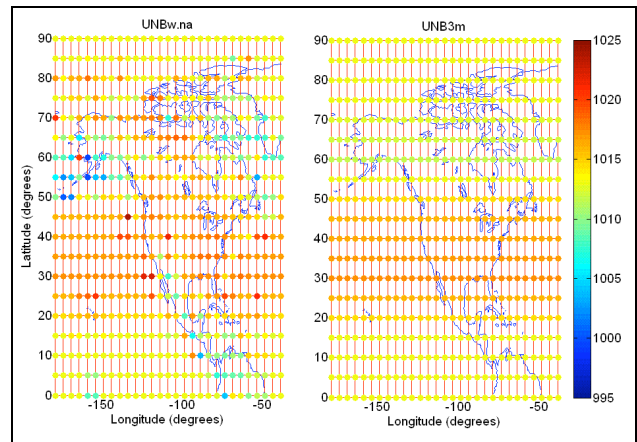


Figure 11. Average pressure at grid nodes, given by UNBw.ca and UNB3m, in mbar.

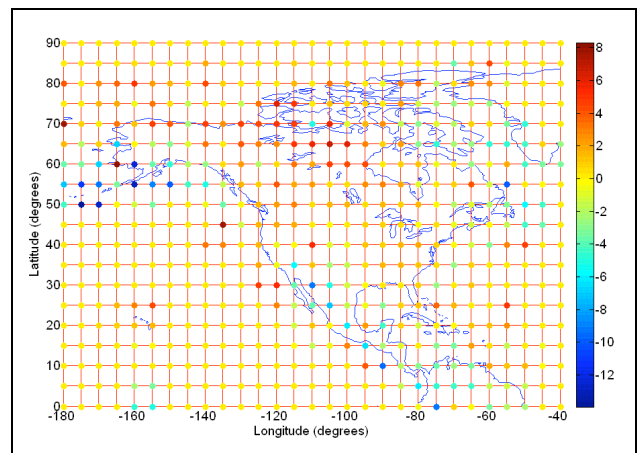


Figure 12. Average MSL pressure difference between UNBw.na and UNB3m, in mbar.

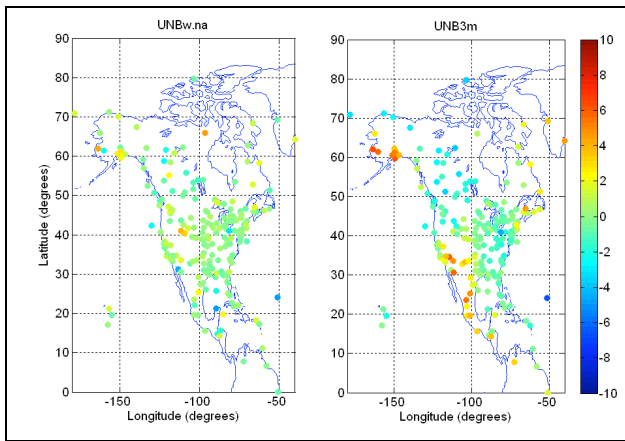


Figure 13. Mean biases encountered when estimating pressure for control stations, in mbar.

The general statistics for pressure estimation are shown in Table 3.

Table 3. General statistics for pressure estimation errors (all values in mbar).

	Bias	Std. Dev.	RMS
UNBw.na	0.05	3.89	3.95
UNB3m	0.02	3.95	4.12

From Table 3 it can be noticed that the differences for bias, standard deviation and rms between the two models are low (considering estimated delays, 1 mbar corresponds to around 2 mm in the zenith direction). Although the general bias of UNBw.na is slightly worse than UNB3m's, UNBw.na's better fitting for different regions is translated into an improvement in standard deviation and rms.

The last step of the model calibration is the relative humidity grid. Following the same procedure as for the other two steps in terms of reporting results, Figure 14 shows the average MSL values of RH (in %) for all grid nodes, given by UNBw.na and UNB3m, where it can be seen that UNBw.na shows a drier area in the southwest part of the continent. This difference can be better visualized in Figure 15, which shows the difference in the average MSL values between the two models for each grid node, in the sense of UNBw.na-UNB3m (in %).

The biases of the water vapour pressure estimation for control stations are shown in Figure 16, where we can notice that UNB3m overestimates the water vapour pressure for the southwest part of the continent, while UNBw.na does not. There is also a region with a small improvement in the northwest part of the continent (is this last case, UNB3m underestimates the WVP).

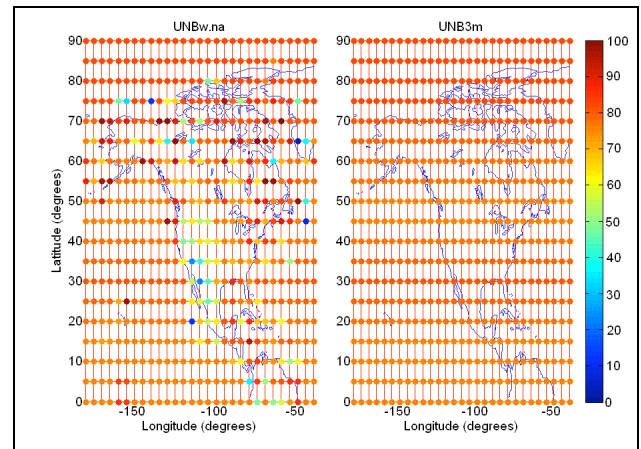


Figure 14. Average MSL relative humidity for grid nodes, given by UNBw.na and UNB3m, in %.

The general performance results can be seen in Table 4, where it can be noticed that there is a significant improvement (around 50%) in bias when estimating surface water vapour pressure with UNBw.na, compared to UNB3m. There is a small improvement in standard deviation, indicating a slightly better fitting to real conditions by UNBw.na.

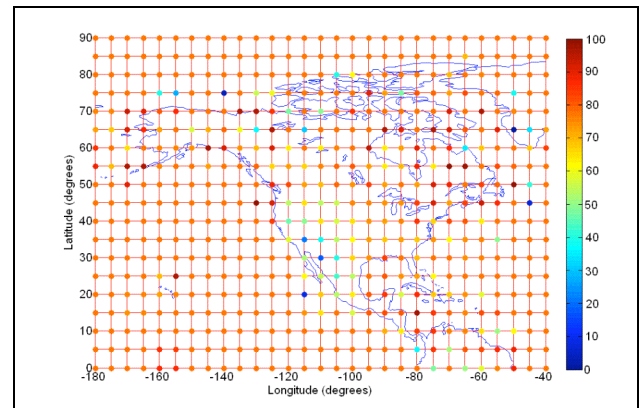


Figure 15. Difference between average MSL relative humidity provided by UNBw.na and UNB3m, in %.

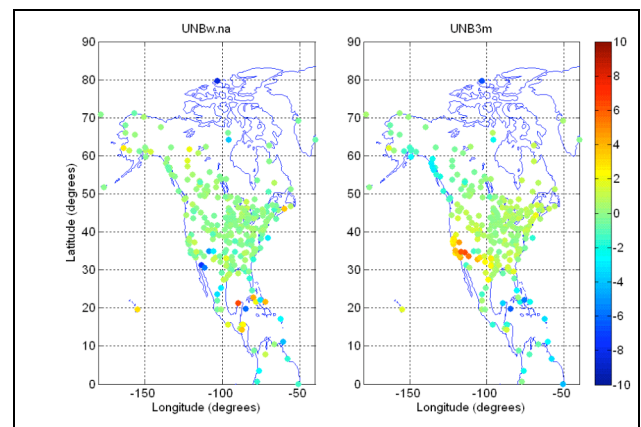


Figure 16. Mean biases encountered when estimating water vapour pressure for control stations, in mbar.

Table 4. General statistics for water vapour pressure estimation errors (all values in mbar).

	Bias	Std. Dev.	RMS
UNBw.na	-0.10	2.30	2.47
UNB3m	0.20	2.43	2.65

### UNBw.na VALIDATION WITH RAY-TRACED DELAYS

In order to verify if UNBw.na is more realistic than UNB3m in terms of delays estimation, a validation process was realized. In this approach radiosonde-derived delays were used as reference (“truth”). The radiosonde profiles of temperature, pressure, and dew point temperature were used to compute zenith delays by means of a ray-tracing technique. We used radiosonde soundings taken throughout North America and some neighboring territories through the years from 1990 to 1996 inclusive. A total of 222 stations were used, distributed as shown in Figure 17.

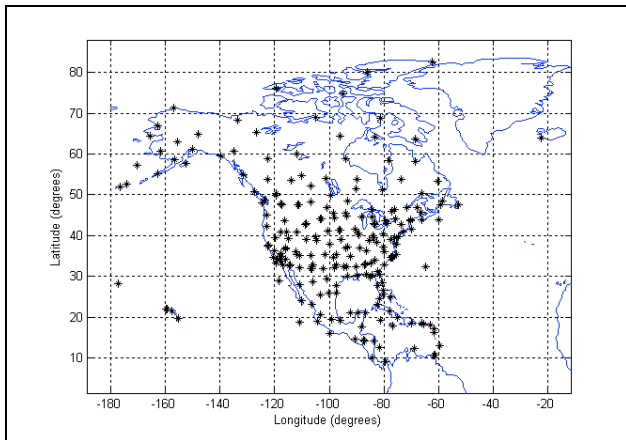


Figure 17. Distribution of radiosonde stations in North America and some nearby territories.

Each station usually has a balloon being launched twice a day, totaling 701,940 soundings for all stations, all years. For each one of the soundings, a total delay was predicted using UNBw.na and UNB3m, and then compared with the ray-traced total zenith delays. From this comparison, bias and rms values could be computed for each one of the stations shown in Figure 17. Figure 18 shows the mean biases found for all stations with the two models.

In Figure 18, the zero value is green according to the color scale. It is possible to notice that the UNBw.na plot shows colors generally closer to green than UNB3m. It can also be noticed that in the western part of the continent, where UNB3m has its worse performance, there is a significant improvement with the new model. The rms values for the same stations can be seen in Figure 19, where it is possible to see that UNBw.na plot presents

colors generally closer to blue (in this plot zero is represented by dark blue), also with a good improvement for the region with worst results provided by UNB3m.

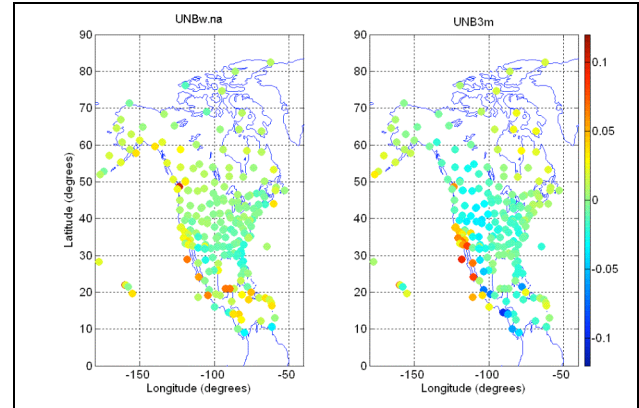


Figure 18. Total zenith delay estimation biases for each station, in meters.

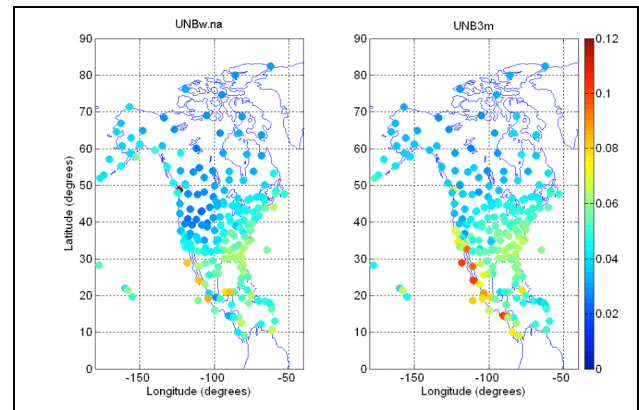


Figure 19. Total zenith delay estimation rms values for each station, in meters.

The general statistics of delay prediction performance of the two models are shown in Table 5, where we can see that there is a general improvement of absolute bias of around 30%, and small improvements in standard deviation (8%) and rms (9%).

Table 5. General statistics of total zenith delay prediction performance (all values in mm).

	Bias	Std. Dev.	RMS
UNBw.na	3.6	44.8	45.0
UNB3m	-5.2	48.9	49.2

Although the general rms doesn't show a significant improvement, the major concern with UNB3m is not its overall performance, but its performance in localized areas. In order to access the performance of the models in different regions, the coverage area was divided into four analysis regions, trying to have approximately the same number of radiosonde stations in each one of them. Figure 20 shows the division of the four regions.

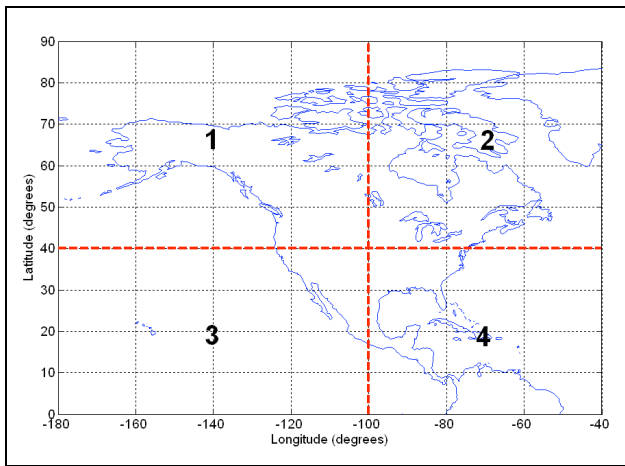


Figure 20. Division of the four analysis regions.

The statistics for each one of the analysis regions are shown in Table 6.

Table 6. Statistics (bias, standard deviation and rms) for analysis regions (all values in cm).

Region	UNBw.na			UNB3m		
	Bias	SD	RMS	Bias	SD	RMS
1	1.0	3.4	3.6	-0.9	3.5	3.7
2	0.4	4.1	4.1	0.5	4.3	4.3
3	0.6	4.4	4.4	0.2	5.7	5.7
4	-0.3	5.4	5.5	-1.3	5.6	5.8

In Table 6 it can be noticed that rms values for UNBw.na are better than UNB3m's for all regions, with a significant improvement for region 3 (around 23%). The bias of region 3 for UNBw.na is higher than for UNB3m, however it does not mean UNB3m is better, because although the mean bias is less, the variation of biases (above and below zero) is much higher than for UNBw.na (as it can be noticed in Figure 18). This effect shows up in UNB3m's standard deviation and rms in region 3, which are significantly higher than UNBw.na's. Another way to show that is by computing the average absolute biases and their standard deviation, computed without considering bias sign. These values are shown in Table 7, where it can be noticed that, indeed, the average absolute bias and its standard deviation is significantly higher for UNB3m in region 3 (UNBw.na shows an improvement of around 25%).

Table 7. Average absolute biases (aab) and their standard deviations (aab-sd) - all values in cm.

Region	UNBw.na		UNB3m	
	aab	aab-sd	aab	aab-sd
1	2.8	2.2	2.8	2.3
2	3.2	2.6	3.4	2.7
3	3.4	2.9	4.5	3.6
4	4.5	3.2	4.7	3.4

One of the problems encountered in UNB neutral atmosphere modes is a systematic behavior with respect to height [Leandro et al., 2006]. In order to verify if the new model has the same problem, Figure 21 shows a plot of station biases with respect to station heights. The error bars are (one sigma) standard deviations of the bias computation for each of the stations, and the red line is the fitted (using the points shown in the plots) linear trend of the models. The upper plot shows results of UNBw.na and the lower one shows UNB3m's results.

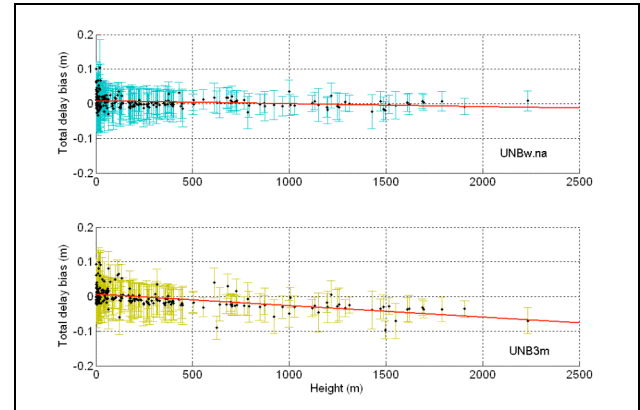


Figure 21. Station biases with respect to station heights.

It can be seen in Figure 21 that UNBw.na does not have a trend as significant as UNB3m, because while UNB3m biases tend to increase negatively as the height goes higher, UNBw.na biases are kept with values around zero no matter the height of the station. This difference can also be clearly seen comparing the two trend lines (red lines) of the models.

In order to visualize the fit of the model estimations to the yearly variation of the zenith total delay, a few stations were selected for analysis.

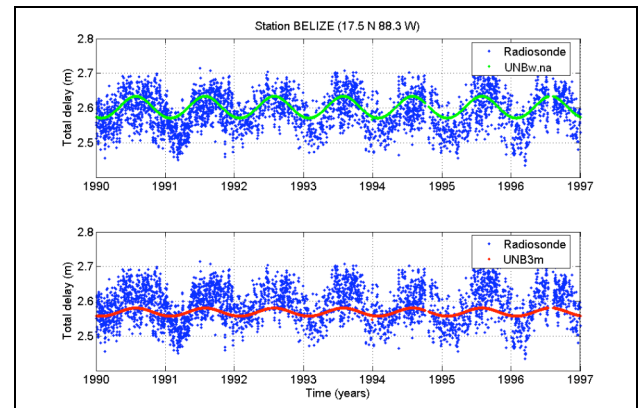


Figure 22. Total zenith delay estimation for station Belize.

The stations selection was based on availability of data for given stations over the period of time of the data set 1990-1996, having sample stations for different latitudes. The chosen stations are Belize, Pittsburgh, Salt Lake City,

Bethel and Eureka. Figures 22 to 26 show the radiosonde ray-traced total zenith delays compared with UNB3m and UNBw.na predictions for each of the stations.

The estimations provided by UNB3m for station Belize have a problem with the annual amplitude of the delays. This effect is caused by the fact that UNB3m assumes that meteorological parameters do not vary over the year for latitudes between 15°N and 15°S. The problem with amplitude underestimation affects even stations at higher latitudes, as in the case of station Pittsburgh. UNBw.na shows a good improvement in terms of estimated annual amplitude, as it can be seen for these two stations.

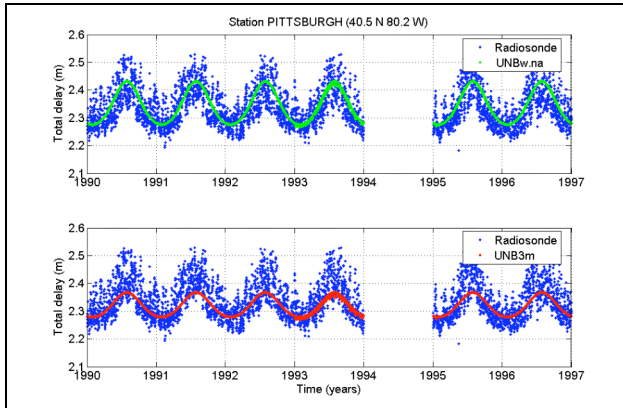


Figure 23. Total zenith delay estimation for station Pittsburgh.

Another problem suffered by UNB3m in the case of Pittsburgh is the underestimation of the delays, which also occurs for Salt Lake City. The average of the delays provided by UNBw.na seem to match much better with ray-traced delays than UNB3m's for these stations.

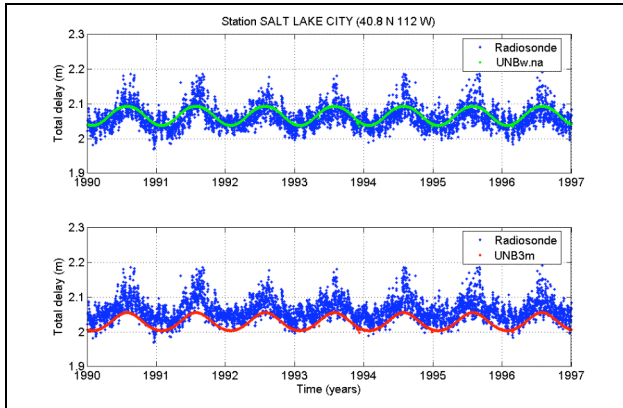


Figure 24. Total zenith delay estimation for station Salt Lake City.

In the case of station Bethel both models seem to work fine, with a good fit with radiosonde-derived delays. However for the northern station, Eureka (80°N), UNB3m predictions are generally overestimating the delays, while

UNBw.na is closer to the average values of the ray-traced delays over the years.

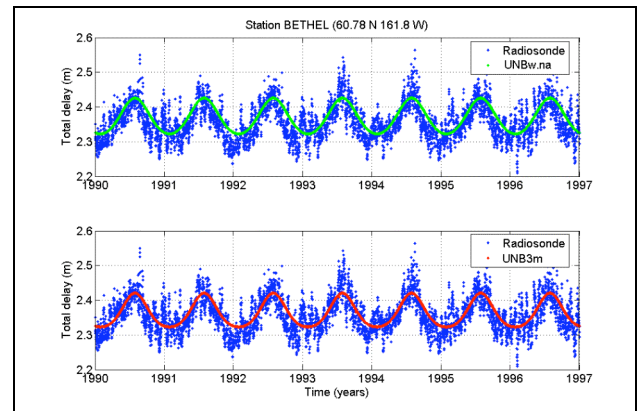


Figure 25. Total zenith delay estimation for station Bethel.

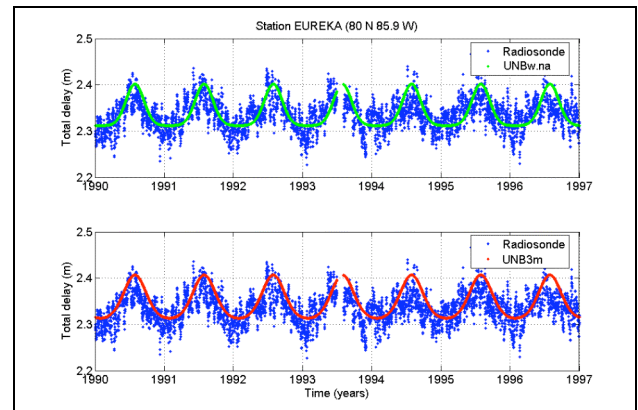


Figure 26. Total zenith delay estimation for station Eureka.

Table 8 shows the numerical results for each of the five stations. With the exception of station Bethel, UNBw.na shows better results for all stations, with improvement of up to 2.8 cm in bias and 1.6 cm in rms (both for station Salt Lake City). If the biases for all stations are considered, it is possible to notice that UNBw.na has more consistent (homogeneous) results for different locations.

Table 8. Numerical results for sample stations (reoriented by the first four characters of their names) – all values in cm.

Station	UNBw.na		UNB3m	
	Bias	RMS	bias	RMS
BELI	1.4	4.7	2.1	5.3
PITT	0.6	4.7	-1.8	5.3
SALT	0.5	2.6	-3.3	4.2
BETH	1.2	3.8	0.6	3.6
EURE	0.5	2.9	1.5	3.2

## CONCLUSIONS AND FUTURE WORK

In this paper an approach for creation of wide area neutral atmosphere models was comprehensively described and discussed. A dataset with hourly surface meteorological measurements was used to create a new model for North America, called here UNBw.na.

The calibration of surface temperature and water vapour pressure lapse rate parameters was performed, and after comparing results of a model calibration with fixed lapse rates it was concluded that better performance is achieved in the second case. One of the reasons behind this conclusion might be the fact that the current dataset (surface meteorological parameters) is not adequate to successfully decorrelate surface lapse rates from actual parameters, due to fact that stations nearby each other tend to have similar heights.

The meteorological values derived from the grids of the new model were compared with actual surface measurements, realized at stations which were not used in the calibration process. All analyses took into consideration the most recent version of UNB models, until now UNB3m.

Results for all three meteorological parameters showed that a grid-based model could perform better than a latitude (only) based model (such as UNB3m). The reason for that is the capability of accommodating longitude or regional climatic characteristics of the continent. In terms of temperature the general bias was practically eliminated, with a reduction of 91% (-0.68 to 0.06 K), while rms was improved by 15% (6.8 to 5.8 K). Pressure estimations were also improved in the new model, with a reduction of more than 50% in bias (0.05 to 0.02 mbar) and a slight improvement in rms (4.12 to 3.95 mbar). Water vapour pressure predictions had their general bias reduced 50% (0.2 to -0.1 mbar), also with slight improvement in rms (2.65 to 2.47 mbar). Although the general results do not show a spectacular improvement, the new model is consistently better than its predecessor, and, the improvement for certain regions is more significant than others. Regions where the performance of the old model was not satisfactory had results significantly improved with the new model.

A validation of UNBw.na predicted zenith delays was realized using radiosonde-derived delays as reference. Soundings carried out throughout North America and some neighboring territories through the years from 1990 to 1996 inclusive were used in this analysis, totaling 222 stations. General results from this analysis showed a general improvement of bias of around 30%, and small improvements in standard deviation (8%) and rms (9%).

Because the main goal with the new model is predicting zenith delays with a consistent uncertainty for different areas, the continent was divided into four analysis regions. This was done to detect localized improvements when using UNBw.na. This analysis showed that all regions manifested improvement for the estimations with the new model.

A problem with systematic behavior of biases (of zenith delay estimation) with height which has been previously detected in UNB neutral atmosphere models no longer exists in UNBw.na. Biases were shown to be consistently close to zero, no matter the height of the station.

Investigation of the performance of both models (UNBw.na and UNB3) with radiosonde ray-raced delays at a few sample stations showed that UNBw.na generally has a better fit to the yearly behavior of the zenith delays. It was also possible to notice that results from UNBw.na are more consistent between stations at different locations than when using UNB3m.

In terms of general conclusions, UNBw.na was shown to be consistently better than UNB3m in several aspects. The adopted procedure for the grid calibration worked in an adequate way, resulting in a reliable model.

Future work involve investigation of lapse rate parameters, which were not calibrated in this work. The model for delay computation, which has not been modified so far, will also be reviewed. Assimilation of different data, such as numerical weather models or contemporary standard atmospheres, still needs to be investigated.

## ACKNOWLEDGEMENTS

We would like to thank Seth Guttman and his colleagues at NOAA for making the ISH database available to us.

We also would like to thank James Davis, Thomas Herring, and Arthur Niell for the ray-tracing software and Paul Collins for providing the radiosonde quality-control software.

The authors gratefully acknowledge the financial support of the Canadian International Development Agency.

## REFERENCES

COESA (1966). *U.S. Standard Atmosphere Supplements, 1966*. U.S. Committee on Extension to the Standard Atmosphere. Sponsored by Environmental Science Services Administration, National Aeronautics and Space Administration, United States Air Force and published by

the Superintendent of Documents, U.S. Government Printing Office, Washington, D.C.

Collins J.P. and R.B. Langley (1998). “*The Residual Tropospheric Propagation Delay: How Bad Can It Get?*” Proceedings of ION GPS-98, 11th International Technical Meeting of the Satellite Division of The Institute of Navigation, Nashville, TN, 15-18 September 1998, pp. 729-738.

Krueger E, Schüler T, Hein GW, Martellucci A, Blarzino G (2004). “*Galileo tropospheric correction approaches developed within GSTB-VI*”. Proceedings of GNSS 2004—European navigation conference, 17–19 May 2004, Rotterdam, The Netherlands

Leandro R.F., Santos, M.C. and Langley R.B., (2006). *UNB Neutral Atmosphere Models: Development and Performance*. Proceedings of ION NTM 2006, Monterey, California, January, 2006.

McCarthy D.D. and G. Petit (2004). *IERS Conventions (2003)*. IERS Technical Note 32, Verlag des Bundesamts für Kartographie und Geodäsie, Frankfurt am Main.

Niell, A.E. (1996). “Global Mapping Functions for the Atmosphere Delay at Radio Wavelengths.” *Journal of Geophysical Research*, Vol. 101, No. B2, pp. 3227- 3246.